Available online at www.sciencedirect.com
ScienceDirect
Journal of Luminescence 128 (2008) 1331–1338
JOURNAL OF LUMINESCENCE
www.elsevier.com/locate/jlumin

Oxygen-sensing materials based on $[Ru(bpy)_3]^{2+}$ covalently grafted MSU-3 mesoporous molecular sieves

Haoran Zhang[a,b], Bin Li[a,*], Bingfu Lei[a], Wenlian Li[a]

[a]*Key Laboratory of Excited State Processes, Changchun Institute of Optics Fine Mechanics and Physics, Chinese Academy of Sciences, Changchun 130033, China*
[b]*Faculty of Chemistry, Northeast Normal University, Changchun 130024, China*

Received 16 October 2007; received in revised form 1 December 2007; accepted 18 December 2007
Available online 5 January 2008

Abstract

Novel oxygen-sensing materials consisting of $[Ru(bpy)_2(Bpy\text{-}Si)]^{2+}$ portions covalently grafted onto the backbone of MSU-3 mesostructured silica-based network were prepared in a two-step process with the help of P123 surfactant. The 2,2′-bipyridyl covalently grafted with 3-aminopropyltriethoxysilane was used not only as sol–gel precursor but also as the second ligand of the $Ru(bpy)_2Cl_2 \cdot 2H_2O$ complex for the preparation of sol–gel-derived silicates for oxygen-sensing materials. The downward oxygen-sensing Stern–Volmer plots can be attributed to the heterogeneous environment of the luminophore within the MSU-3 silica. The MSU-3 sample obtained at 10 °C showed better oxygen-sensing performance due to its special morphology.

Keywords: Ruthenium complex; Covalent grafting; Oxygen sensor; Mesoporous molecular sieves

1. Introduction

There is growing interest in the construction of photochemical oxygen sensors and this tendency has been greatly stimulated by the environmental pollution problem in the past two decades [1,2]. The advantages of these sensors over the conventional amperometric devices are basically as follows: shorter response time, better sensitivity and selectivity, no O_2 consumption, no poison and no requirement for a reference electrode [3–7]. These sensors are based on the principle that oxygen is a powerful quencher of the luminescent intensity and/or lifetime of the luminescent complexes, and the key factors that favor superior performance include high oxygen permeability in the matrix, the optical properties of the luminescent complex and the locally oxygen-quenching ability of the complex [8]. To date, most phosphorescent transition metal complexes have been used for this application, and among the luminophores used for oxygen sensor, the polypyridyl compounds of Ru(II) and metalporphyrins are the most extensively studied owing to their high quantum yields, large Stokes' shifts, long luminescent lifetimes and high photochemical stability [8–11]. The matrix used to load the luminophore requires high oxygen diffusion coefficient and must be robust with respect to singlet oxygen, which is a by-product of the quenching process. A plethora of methods have been described to immobilize sensing chemistries over the years. Among these reported methods, the sol–gel method has proved to be an efficient technique to prepare optical oxygen-sensing devices due to its many desirable properties such as high thermal stability, good photostability and optical transparency in the visible-light region [12].

To date, most previous work has been done using the physical mixing methods in which only weak interactions exist between the matrix and the luminophore. Unfortunately, the physisorption of the transition metal complex in such two-component systems often results in luminophore aggregation within the matrix and dye leaching when used in liquid environment, which will lead to a serious problem in terms of signal stability and longevity due to the absence of strong covalent interaction between the organic and inorganic constituents [13–15]. Consequently, an attractive

*Corresponding author. Tel./fax: +86 43186176935.
E-mail address: lib020@ciomp.ac.cn (B. Li).

0022-2313/$ - see front matter © 2008 Published by Elsevier B.V.
doi:10.1016/j.jlumin.2007.12.043

approach used to overcome the above-mentioned drawbacks was to chemically bond the organic and inorganic portions via the powerful covalent bonds such as Si–CH_2 [12,16–23]. In addition, the incorporation of oxygen-sensing complexes into the mesoporous molecular sieves have proved to be a successful method to increase their sensitivity because their special pore structure favors the diffusion of analyte within the porous channel [8,12,22].

In this work, the MSU-3 mesoporous molecular sieve is used as the inorganic support to covalently graft the ruthenium polypyridyl complexes via the Si–CH_2 bonds for oxygen sensor. It is expected that the MSU-3 mesoporous molecular sieves will possess certain interesting characteristics when used for oxygen sensors. As the microstructure of the MSU-type mesoporous molecular sieve is greatly dependent on the synthesis temperature, Ru(II) covalently grafted MSU-3 silica prepared under different temperatures were prepared. The oxygen-sensing performances of all samples were discussed based on the luminescence intensity quenching. The results found that the MSU-3 obtained at 10 °C with spherical morphology has the best oxygen-sensing performance.

2. Experimental

2.1. Chemicals and procedures

The 4,4′-dimethyl-2,2′-dipyridyl, Pluronic (P123), and 3-aminopropyltriethoxysilane (APS) were obtained from Aldrich (Milwaukee, WI, USA) and were used without further purification. The tetraethoxysilane (TEOS) was purchased from Tianjin Chemical Company. The concentrated HCl, sulfuryl dichloride ($SOCl_2$, A. R.) and EtOH were obtained from Shanghai Chemical Company. $SOCl_2$ was used after distillation in vacuo. The complex bis(2,2′-bipyridyl) ruthenium(II) chloride, $Ru(bpy)_2Cl_2$ was synthesized and purified as described in Ref. [24]. The water used in our present work was de-ionized.

The ligand denoted as Bpy-Si was prepared according to a literature procedure [15,18,20,21]. To obtain the hydrolysable $Ru(bpy)_2(Bpy\text{-}Si)Cl_2$, a mixture of $Ru(bpy)_2Cl_2$ and Bpy-Si (mole ratio of Bpy-Si/$Ru(bpy)_2Cl_2$ was 1.02) in anhydrous ethanol was refluxed for 8 h in nitrogen atmosphere to obtain a transparent deep-red solution, indicating that the complexation reaction between Bpy-Si and $Ru(bpy)_2Cl_2$ was complete. Finally the ethanol was rotary evaporated off and the residue was washed with ether and acetone for several times, and dried in vacuo.

MSU-3 hexagonal mesoporous materials were prepared according to the two-step reaction process [25]. In a typical synthesis, 1.5 g (2.58×10^{-3} mol) of P123 was dissolved in 100 mL of de-ionized water previously acidified at pH = 2 with concentrated hydrochloric acid. After full dissolution, 0.0363 g $Ru(bpy)_2(Bpy\text{-}Si)Cl_2$ and 7.37 ml (0.032 mol) TEOS (Ru/TEOS = 0.1%) were added at room temperature under moderate magnetic stirring for 2 h. After 12 h of aging at room temperature without stirring, this solution was monitored to desired temperature (10, 45 and 65 °C) and the final condensation step was induced by the addition of 5.1 mL of sodium fluoride (0.25 M) (NaF/TEOS = 4%) into the solution kept in a thermostated stirring bath for 3 days. The final product was filtered off and washed with water, and air-dried at 50 °C. Removal of surfactant P123 was conducted by Soxhlet extraction with ethanol under reflux for 24 h.

2.2. Instruments and measurements

FT-IR spectra were measured within the 4000–400 cm^{-1} region on an infrared spectrophotomer (Model Perkin-Elmer Model 580B) with a resolution of $\pm 4\,cm^{-1}$ using the KBr pellet technique. Photoluminescence spectra of these samples were determined with a Hitachi F-4500 fluorescence spectrophotometer equipped with a monochromator (resolution: 0.2 nm) and a 150 W Xe lamp as the excitation source, whose excitation and emission slits were 5 and 5 nm, respectively.

The oxygen-sensing properties of our present samples were discussed based on the fluorescence intensity. For the Stern–Volmer plots measurement, oxygen and nitrogen were mixed at different concentrations via gas flow controllers and passed directly to the sealed gas chamber. We typically allowed 1 min between changes in the N_2/O_2 concentration to ensure that a new equilibrium point had been established [12,22]. Equilibrium was evident when the luminescence intensity remained constant ($\pm 2\%$). The sensing response curves were obtained using the same method.

The unquenched excited-state lifetimes of MSU-3 mesoporous samples at nitrogen conditions were measured using a conventional Nd:YAG (neodymium:yttrium aluminum garnet) laser system (Spectra Physics) as described in Refs. [12,22].

3. Results and discussion

According to Li et al. [18] and Malins et al.'s [15] work, we have successfully chemically grafted the 2,2′-bipyridyl to 3-aminopropyltriethoxysilane to obtain the grafted hydrolysable precursor (Bpy-Si) [21]. This compound has terminal silanol groups that can proceed with a polycondensation reaction with the TEOS under acidic catalytic conditions. It is well understood that the hydrolysis and polycondensation reactions between the Bpy-Si and TEOS will succeed in covalently grafting the silicates backbone. The FT-IR spectrum has proved the successful formation of the covalent grafting between the organic and inorganic components in this system.

The presence of organic ligands covalently bonded to the network of MSU-3 mesoporous silicate is characterized by FT-IR. The FT-IR spectra of the hydrolysable Ru$(bpy)_2(Bpy\text{-}Si)Cl_2$ complex (a) and the final obtained Ru(II) covalently grafted MSU-3 sample (b) are shown in Fig. 1. In Fig. 1a, the spectrum of $Ru(bpy)_2(Bpy\text{-}Si)Cl_2$ is

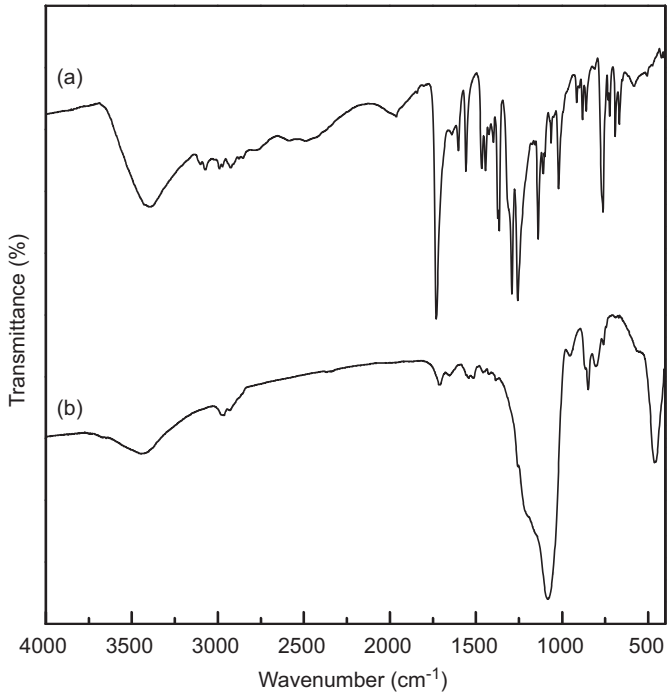

Fig. 1. FT-IR spectra of (a) hydrolysable $Ru(bpy)_2(Bpy\text{-}Si)Cl_2$ complex and (b) the finally obtained MSU-3 oxygen-sensing material.

dominated by ν (C–Si, 1203 cm^{-1}) and ν (Si–OEt, 1076 cm^{-1}) absorption bands, which are the characteristics of trialkoxylsilyl functions. The bending vibration of Si–O at 462 cm^{-1} from APS is obvious in Fig. 1a, indicating that the APS has been successfully grafted onto 2,2′-bipyridine [21]. In panel b of Fig. 1, the formation of the Si–O–Si framework is evident by the bands located at 1084 cm^{-1} (ν_{as}, Si–O), 802 cm^{-1} (ν_s, Si–O) and 456 cm^{-1} (δ, Si–O–Si) (ν represents stretching, δ in-plane bending, s symmetric, and as asymmetric vibrations) [20,21]. The peaks at 1656 and 1636 cm^{-1}, originating from the CONH group of Bpy-Si, can also be observed in the as-synthesized material, which is consistent with the fact that the Bpy-Si group in the framework remains intact after the hydrolysis/condensation reaction. The broad absorption band at 1120–1000 cm^{-1} corresponding to the ν (Si–O–Si), as shown in Fig. 1b, indicates the formation of siloxane network. The introduction of TEOS and water to the $Ru(bpy)_2(Bpy\text{-}Si)Cl_2$ results in the changes in the IR spectra due to the hydrolysis/condensation of TEOS and $Ru(bpy)_2(Bpy\text{-}Si)Cl_2$. The remaining ν(Si–C) vibration located at 1208 cm^{-1} indicates that no (Si–CH_2) bond cleavage occurs during the hydrolysis/condensation reactions.

We have performed small-angle X-ray scattering diffraction (SAXRD) experiments of the MSU-3 mesostructured silicates prepared at different temperatures after surfactant extraction to gain insight into the structure of these oxygen-sensing materials. Their SAXRD patterns are shown in Fig. 2, which exhibit great differences, and the specific features that make their structure sensitive to

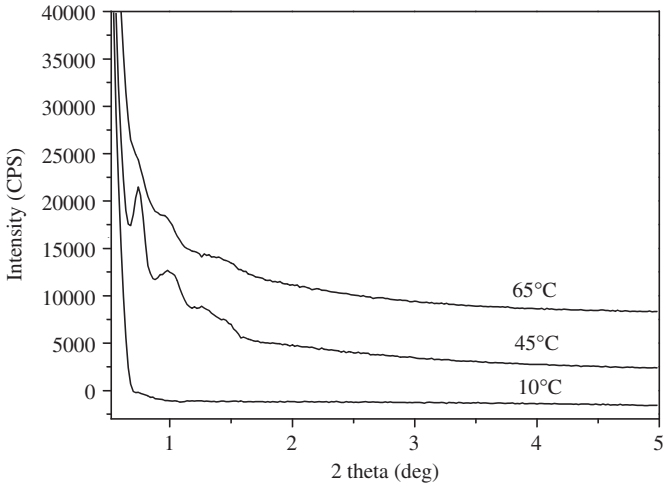

Fig. 2. XRD patterns of extracted Ru(II)-MSU-3 materials prepared at different temperatures.

synthesis temperature have been discussed in detail by Martines et al. [26] previously. The SAXRD patterns in our present work are consistent with the previous reports [25,26]. The particles morphology is extremely dependent on the synthesis temperature and three domains can be discriminated: below 25 °C, the particles exhibit a spherical shape; from 35 to 45 °C, the powder is totally made of stick-like particles; and above 45 °C, the particles lose their structure and evolve toward a fluffy powder with a growing amorphous part made of very small aggregates of silica. From an amorphous state (below 25 °C) to another amorphous state (above 45 °C) there is a long-range order described by a three-dimensional (3D) wormhole structure. As shown in Fig. 2, the sample synthesized at 45 °C exhibits diffraction peaks that can be assigned to a hexagonal symmetry. The main peak points out at 0.74° can be assigned to the d_{100} reflection. The other two peaks located at 0.99° and 1.26° may be assigned to the d_{110} and d_{200} reflections, respectively.

Fig. 3 shows the representative nitrogen adsorption/desorption isotherms of the surfactant-extracted undoped MSU-3 silica and the Ru(II) covalently grafted MSU-3 sample prepared at 45 °C. The isotherm patterns exhibit hysteresis, characteristic of pore necking, and the adsorption increases at high relative pressure, characteristic of the textural porosity. It can be concluded that the microstructure of the Ru(II) covalently grafted MSU-3 prepared at 45 °C has a 3D shape with stick-like mesoporous channels inside, which are connected through pore necklings, and the cross-sections of the stick-like channel have hexagonal symmetry. The pore size distribution inserted in Fig. 3 indicates that the Ru(II) covalently grafted MSU-3 sample possesses obviously narrower pore size distribution than the empty MSU-3 sample, with mean pore diameters equal to 3.9 and 8.4 nm for the former and the latter, respectively. So we suppose that the Ru(II) complex sections have been covalently grafted onto the backbone of the mesoporous silica. The successful covalent grafting

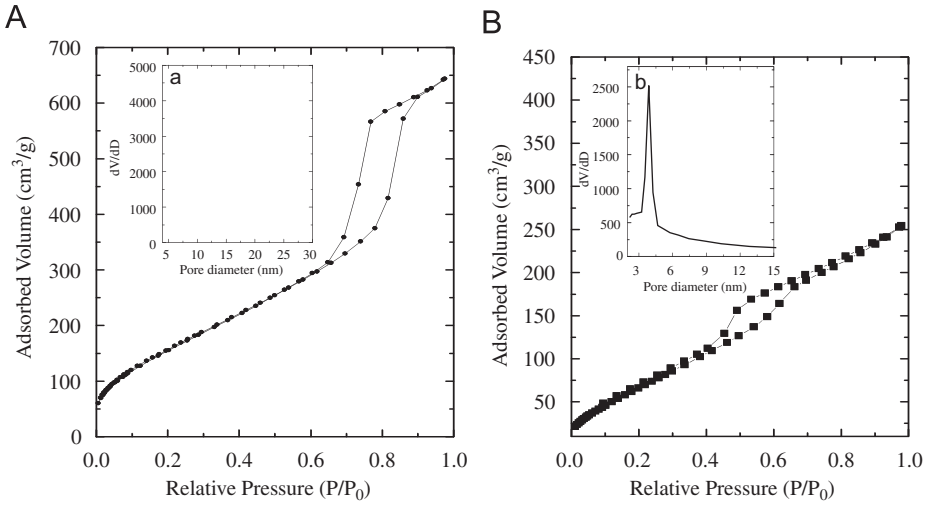

Fig. 3. Nitrogen adsorption/desorption isotherms of (A) the surfactant-extracted undoped MSU-3 silica and (B) the Ru(II) covalently grafted MSU-3 sample prepared at 45 °C. The insets are their pore size distributions.

of the Ru(II) complex onto the silicate backbone can be further proven by the blue-shift of the maximum emission of Ru(II) complex from 646 to 601 nm when the complex is immobilized within the MSU-3 matrix obtained at 45 °C. This blue-shift is probably caused by the change of the MLCT excited state within the silicate during the formation of the Si–O network structure. Such a blue-shift can be explained on the basis of the suppression of the vibrational deactivation and the restriction on the mobility of the Ru(II) complex in an excited state due to the rigidity of the silica matrix [27].

As mentioned above, the Ru(II) complex optical sensors are based on the principle that oxygen is a powerful quencher of their luminescent intensity and/or lifetime. In homogeneous media with a single-exponential decay, the intensity and lifetime forms of the Stern–Volmer equation with dynamic quenching are as follows [3,12,22]:

$$I_0/I = \tau_0/\tau = 1 + K_{SV} pO_2 = 1 + \kappa\tau_0 pO_2, \quad (1)$$

where I and τ are, respectively, the fluorescence intensity and excited-state lifetime of the luminophore, the subscript 0 denotes the absence of oxygen, K_{SV} is the Stern–Volmer constant, κ is the bimolecular rate constant, and pO_2 is the partial pressure of oxygen at 1 atmosphere pressure. However, when the Ru(II) complex is located in a microscopic-scale heterogeneous matrix, the linear Stern–Volmer quenching curves in Eq. (1) should be recast as follows [3,7,12,13,22,27,28]:

$$\frac{I_0}{I} = \frac{1}{f_{01}/(1 + K_{SV1} pO_2) + f_{02}/(1 + K_{SV2} pO_2)}, \quad (2)$$

where f_{0i} valuables are the fraction of each of the two sites contributing to the unquenched intensity, K_{SVi} values are the associated Stern–Volmer quenching constants for the two sites. Eq. (2) is the familiar Demas "two-site" model that has been proven to have excellent ability to describe the nonlinear Stern–Volmer quenching curves [3,12,13,22,28]. It is not surprising given the well-known ability of two exponentials to give excellent fits to complex decay curves, which are made up of the distribution function of exponential decays. In the case where one fraction of the luminophore is nonquenchable ($K_{sv2} = 0$), Eq. (2) collapses to another similar Lehrer expressed as shown in Eq. (3) [29]. The previous reported results revealed that the Lehrer model can also be used to give excellent fit to the downward Stern–Volmer plots [3,22,29,30]:

$$\frac{I_0}{I} = \frac{f_{01}}{1 + K_{SV1} pO_2} + f_{02}. \quad (3)$$

In these above-mentioned Lehrer and Demas two-site models, there are at least two excited-state lifetime components for the luminescence species because they are located at microheterogeneous microenvironments. In this case, their excited-state lifetime decay analysis may be described by

$$I(t =)\alpha_1 \exp(-t/\tau_1 +)\alpha_2 \exp(-t/\tau_2), \quad (4)$$

where $I(t)$ represents the fluorescence intensity at time t, the subscripts 1 and 2 denote the assigned lifetime components, and α_i denotes the pre-exponential factors. The weighted mean lifetime τ_m can be calculated by [31]

$$\langle\tau_m\rangle = \sum_{i=1}^{2} \alpha_i\tau_i \Big/ \sum_{i=1}^{2} \alpha_i. \quad (5)$$

It should be noted that sufficient removal of surfactant P123 is necessary to obtain better oxygen-sensing performances because the surfactant located on the silicate surface of the MSU-3 sample would inevitably prevent the luminescent Ru(II) complex from colliding with the oxygen molecule. This assumption has been proved by the fact that the as-prepared sample without extraction of surfactant does not show any obvious oxygen-sensing properties. Fig. 4 presents the intensity-based Stern–Volmer plots for Ru(II) covalently grafted MSU-3 mesostructure silicates obtained at different temperatures. For comparison, the simply

physisorbed sample prepared at 10 °C is also prepared and its Stern–Volmer plot is shown as curve d of Fig. 4. Inspection of these results in Fig. 4 reveals that all samples possess a downward curvature. The downward curvatures of the Stern–Volmer plots are fully in line with the behavior of a wide variety of luminophore-doped sol–gel-derived xerogels [3,12,22,28,31]. This kind of nonlinearity in the Stern–Volmer plot is associated with the luminophore molecules being distributed simultaneously between two or more sites within the sol–gel-derived silicate in which one site is more heavily quenched than the other. For this kind of microheterogeneous solid-based oxygen sensors, it is worth noting that either the Demas two-site model or the Lehrer model can be used to fit the intensity–quenching curves of all of these samples [3,12,13,22,28]. The fitting parameters in Table 1 represent the best fits to the curves in Fig. 4. It is reasonable to explain the downward Stern–Volmer plots of all the covalently grafted Ru(II)-MSU-3 samples when the matrix structural features are taken into consideration. A peculiar character of nonionic triblock copolymer surfactant should be addressed that they are able to penetrate into the silica wall [22], which leads to the emergence of the micropores between the mesopores. The MSU-3 materials consist of mesopores that are interconnected by micropores in the pore walls, then heterogeneous environments for the luminophore are present within the MSU-3 silica. The Ru(II) complex located at different microenvironments possesses different oxygen-quenching ability, which consequently results in the downward curvatures of the Stern–Volmer plots.

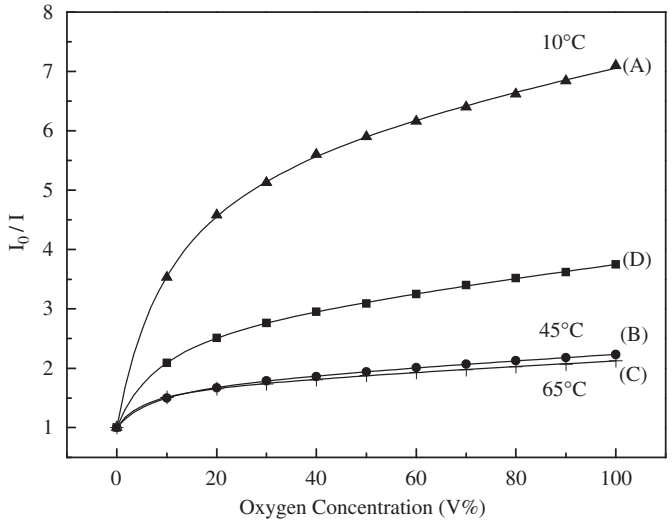

Fig. 4. The Stern–Volmer plots of surfactant-extracted Ru(II) covalently grafted MSU-3 samples obtained at different temperatures: (A) 10 °C; (B) 45 °C and (C) 65 °C; and the surfactant-extracted Ru(II) simply physisorbed MSU-3 sample obtained at 10 °C given for comparison (D). The solid lines represent the best-fit using the Demas two-site model Eq. (2).

Another feature observed from the Stern–Volmer plots is that the sensitivity (I_0/I) of the sample prepared at 10 °C is obviously higher than others. We attribute the higher sensitivity to the spherical micromorphology of the MSU-3 obtained at 10 °C [25,26], which possess the largest surface areas and the portion of functional molecules Ru(II) complex that covalently grafted onto the backbone, and this feature can improve the locally oxygen-quenching ability of the luminophore, as shown by the higher K_{sv} values in Table 1. The Ru(II) covalently grafted sample obtained at 10 °C possesses higher sensitivity compared with the Ru(II) simply physisorbed sample obtained at 10 °C, as shown in curves a and d of Fig. 4. We attribute this result to the fact that the Si–CH_2 covalent bonds between the Ru(II) complex and the silicate backbone have improved the distribution of luminophore and prevent them from agglomerating. This result is consistent with that of our previous reports [12,22].

The microscopic-scale heterogeneous local environment of the Ru(II) complex in the MSU-3 samples can be further confirmed by the time-resolved intensity decay curves as shown in Fig. 5. The unquenched lifetimes of different MSU-3 oxygen-sensing materials measured under N_2 atmosphere are tabulated in Table 2. Furthermore, the contents of the Ru(II) ions in different MSU-3 samples are performed by ICP-AES measurements, and the contents are also listed in Table 2. All of the data present in Fig. 5 can be well fit by the double-exponential Eq. (4), which confirms the above-mentioned assumption that the Ru(II) ions occupy not only a homogeneous average local

Table 1
Intensity-based Stern–Volmer oxygen quenching fitting parameters of the different MSU-3 oxygen-sensing materials employing different models, i.e., Demas two-site model and Lehrer model

Samples	I_0/I_{100}	Demas two-site model[a]				Lehrer model[b]		
		K_{SV1} ($O_2\%^{-1}$)	K_{SV2} ($O_2\%^{-1}$)	f_{01}	r^2	K_{SV1} ($O_2\%^{-1}$)	f_{01}	r^2
A	7.1	0.5583±0.0180	0.0024±0.0002	0.84±0.01	0.9998	0.3999±0.02411	0.88±0.01	0.9952
B	2.23	0.2263±0.0111	0.0027±0.0001	0.46±0.01	0.9998	0.1001±0.0102	0.60±0.01	0.9883
C	2.13	0.3084±0.0166	0.0025±0.0001	0.43±0.01	0.9999	0.1182±0.0145	0.56±0.01	0.9839
D	3.75	0.3252±0.0119	0.0034±0.0002	0.67±0.01	0.9999	0.1734±0.0153	0.77±0.01	0.9901

[a]Terms are from Eq. (2). $f_{01}+f_{02}=1$.
[b]Terms are from Eq. (3). f_{01} is the fraction luminophore that is quenchable. K_{SV1} is the Stern–Volmer quenching constant of luminophore that is quenchable. $K_{SV2}=0$.

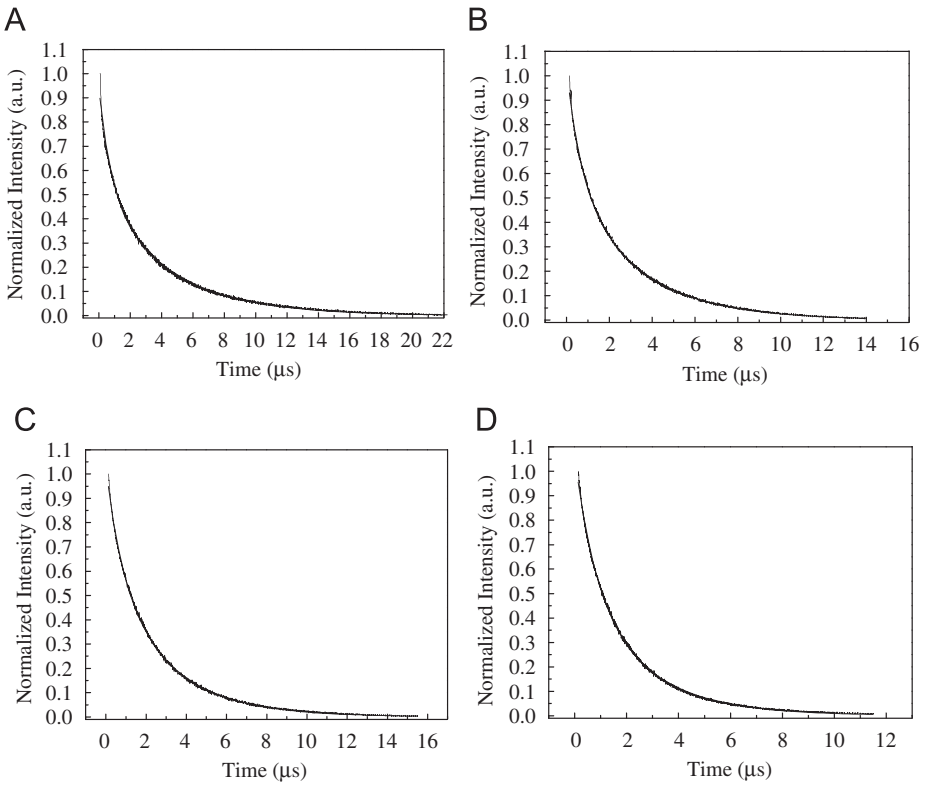

Fig. 5. Typical time-resolved intensity decay curves of different functionalized MSU-3 oxygen-sensing materials: (A) Ru(II) covalently grafted MSU-3 obtained at 10 °C; (B) Ru(II) covalently grafted MSU-3 obtained at 45 °C; (C) Ru(II) covalently grafted MSU-3 obtained at 65 °C; and (D) Ru(II) simply physisorbed MSU-3 sample obtained at 10 °C given for comparison.

Table 2
Content of Ru(II) and time-resolved intensity decay curves constants of the functionalized mesostructured MSU-3 oxygen-sensing materials covalently grafted or physically incorporated with the Ru(II) complex

Sample	$t\downarrow$ (s)	$T\uparrow$ (s)	Ru(II) content[a] (mg/g)	α_1	τ_1 (μs)	α_2	τ_2 (μs)	$\langle\tau\rangle^b$ (μs)	r^2
A	3.0	21.0	0.055	0.41	0.77	0.53	4.32	2.88	0.9982
B	3.0	29.0	0.057	0.26	0.67	0.36	3.12	2.10	0.9991
C	5.0	27.5	0.070	0.40	0.79	0.64	2.86	2.07	0.9993
D	7.5	33.5	0.042	0.10	0.76	0.13	2.37	1.66	0.9993

[a]The contents of the Ru(II) complex in weight (mass %) according to the weight of the final obtained product.
[b]The lifetime measurements are performed under unquenched conditions (N_2) and calculated by Eq. (5).

environment but also a different microheterogeneous local environment within the functionalized mesoporous MSU-3 matrix. As aforementioned, it is reasonable to explain the microheterogeneous local environment of all these functionalized MSU-3 samples when their structural features are taken into consideration. The porous structure of MSU-3 consists not only of large, uniform, and ordered mesopores, but also of much smaller complementary micropores that provide connectivity between the ordered mesopores [22,32,33]. Consequently, the microheterogeneous Ru(II) distribution results in the obvious downward curvature of the Stern–Volmer plots as shown in Fig. 4. As shown in Table 2, lifetime values can be measured from the physisorbed sample compared with those covalently grafted samples despite their similar Ru(II) contents. This result can be attributed to the fact that the physisorbed sample possesses larger amounts of –OH group in the mesoporous channel surface compared with that of the covalently grafted functionalized sample where surface –OH groups have been partly replaced by the luminophore [22].

The reversibility and reproducibility of the oxygen-sensing signal are crucial parameters when periodically repeatedly exposed to pure N_2 and O_2 atmosphere under excitation. From Fig. 6, we can see that the sample prepared at 10 °C possesses the best response signals, and has the shortest response time (denoted as $t\downarrow$, 3 s) when changing from 100% N_2 to 100% O_2 and the shorter recovery time (denoted as $t\uparrow$, 21 s) when from 100% O_2 to 100% N_2. The short response time of the MSU-3 samples is

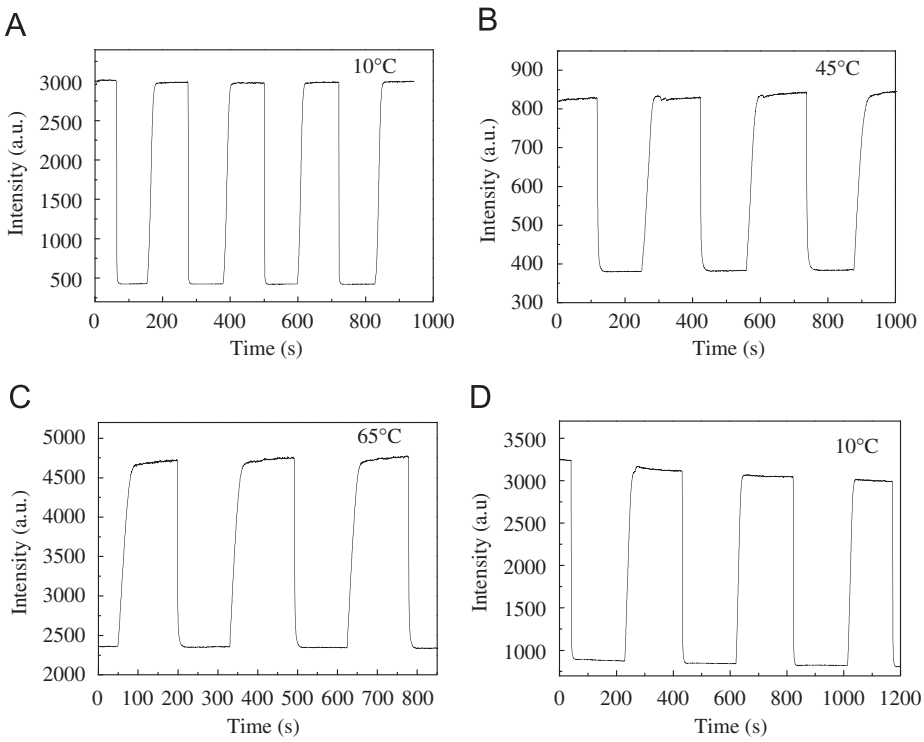

Fig. 6. Relative intensity change and reproducibility of surfactant-extracted Ru(II) covalently grafted MSU-3 samples prepared at different temperatures when exposed to alternate environments of 100% nitrogen and 100% oxygen: (A) 10 °C; (B) 45 °C; and (C) 65 °C; and the surfactant-extracted Ru(II) simply physisorbed MSU-3 sample obtained at 10 °C given for comparison (D).

because the mesoporosity of the matrix favors the oxygen diffusion, which results in quick oxygen quenching. These results furthermore indicate that the micromorphology of the matrix can affect the oxygen-sensing performances to a certain extent, which is consistent with the above-mentioned Stern–Volmer plots results. The Ru(II) simply physisorbed sample (D) shows obvious photobleaching effect under irradiation within the time frame of the measurement. This photobleaching phenomenon is very frequently encountered in other metal complex-doped hybrid materials in which only weak physical interactions exist between the dopants and the matrix [22,34]. However, the other three Ru(II) covalently grafted samples are more stable because of the existence of strong Si–CH_2 bonds between the inorganic and the organic components. This is to say, the Si–CH_2 bonds can effectively significantly limit the vibrations of the Ru(II) complex under irradiation. The improvement of photostability under light irradiation is a crucial aspect for practical applications.

4. Conclusion

This paper presents the synthesis of covalent-grafted Ru(II)-MSU-3 silica through the two-step process that involves the preliminary preparation of stable hybrid micelles that allowed us to modify its microstructure through the monitoring of the synthesis temperature. It appears that the sample prepared at low temperature (10 °C) favors the better sensing properties because its spherical morphology possesses the largest surface areas and the Ru(II) molecules covalently grafted onto the silica backbone. The covalently grafted samples show good reversible signals. This result sets a basis for the microstructure choice of sensing materials in future observations. The oxygen-sensing properties of this new kind of covalently grafted functionalized mesoporous materials can be further improved via changing the microstructure of the sensor supports, and further work is in progress. Furthermore, the covalent grafting strategy reported in this article allows one to extend this method to prepare other organometallic complex-doped devices with better performance.

Acknowledgments

The authors gratefully thank the financial supports of One Hundred Talents Project from Chinese Academy of Sciences, and the National Natural Science Foundations of China (Grant no. 20571071).

References

[1] K. Matsui, F. Momose, Chem. Mater. 9 (1997) 2588.
[2] D.S. Tyson, J. Bialecki, F.N. Castellano, Chem. Commun. (2000) 2355.
[3] Y. Tang, E.C. Tehan, Z. Tao, F.V. Bright, Anal. Chem. 75 (2003) 2407.
[4] A. Mills, C. Tommons, R.T. Bailey, M.C. Tedford, P.J. Crilly, Analyst 131 (2006) 495.

[5] R.M. Bukowski, R. Ciriminna, M. Pagliaro, F.V. Bright, Anal. Chem. 77 (2005) 2670.
[6] A. Mills, Analyst 124 (1999) 1301.
[7] A. Mills, M. Thomas, Analyst 122 (1997) 63.
[8] H. Zhang, Y. Sun, K. Ye, P. Zhang, Y. Wang, J. Mater. Mater. 15 (2005) 3181.
[9] Z. Wang, A.R. McWilliams, C.E.B. Evans, X. Lu, S. Chung, M.A. Winnik, I. Manners, Adv. Funct. Mater. 12 (2002) 415.
[10] R. Ramanoorthy, P.K. Dutta, S.A. Akbar, J. Mater. Sci. 38 (2003) 4271.
[11] S.M. Borisov, V.V. Vasil'ev, J. Anal. Chem. 59 (2004) 176.
[12] B. Lei, B. Lin, H. Zhang, S. Lu, Z. Zheng, W. Li, Y. Wang, Adv. Funct. Mater. 16 (2006) 1883.
[13] E.R. Carraway, J.N. Demas, B.A. DeGraff, J.R. Bacon, Anal. Chem. 63 (1991) 337.
[14] X. Lu, M.A. Winnik, Chem. Mater. 13 (2001) 3449.
[15] C. Malins, S. Fanni, H.G. Glever, J.G. Vos, B.D. MacCraith, Anal. Commun. 16 (1999) 3.
[16] C. Sanche, F. Ribot, New. J. Chem. 18 (1994) 1007.
[17] D. Dong, S. Jiang, Y. Men, X. Ji, B. Jiang, Adv. Mater. 12 (2000) 646.
[18] H.R. Li, J. Lin, H.J. Zhang, H.C. Li, L.S. Fu, Q.G. Meng, Chem. Commun. (2001) 1212.
[19] A.C. Franville, D. Zambon, R. Mahiou, Y. Troin, Chem. Mater. 12 (2000) 428.
[20] H. Zhang, Y. Bai, B. Li, B. Lei, C. Fu, Chem. J. Chin. Univ. 28 (2007) 16.
[21] H.R. Zhang, B. Li, B.F. Lei, W.L. Li, S.Z. Lu, Sensors Actuators B 123 (2007) 508.
[22] B. Lei, B. Li, H. Zhang, L. Zhang, W. Li, J. Phys. Chem. C 111 (2007) 11291.
[23] H.R. Zhang, B. Li, B.F. Lei, W.L. Li, Chem. J. Chin. Univ. 28 (2007) 1920.
[24] G. Sprintschnik, H.W. Sprintschnik, P.P. Kirsch, D.G. Whitten, J. Am. Chem. Soc. 99 (1977) 4947.
[25] C. Boissière, A. Larbot, A. van der Lee, P.J. Kooyman, E. Prouzet, Chem. Mater. 12 (2000) 2902.
[26] M.A.U. Martines, E. Yeong, A. Larbot, E. Prouzet, Micro. Meso. Mater. 74 (2004) 213.
[27] P. Innocenzi, H. Kozuka, T. Yoko, J. Phys. Chem. B 101 (1997) 2285.
[28] M.T. Murtagh, M.R. Shahriari, M. Krihak, Chem. Mater. 10 (1998) 3862.
[29] S.S. Lehrer, Biochemistry 10 (1970) 3254.
[30] I. Klimant, F. Ruckruh, G. Liebsch, A. Stangelmayer, O. Wolfbeis, O. Mikrochim, Acta 131 (1999) 35.
[31] L. Sacksteder, J.N. Demas, B.A. DeGraff, Anal. Chem. 65 (1993) 3480.
[32] M. Hartmann, A. Vinu, Langmuir 18 (2002) 8010.
[33] S. Jun, S.H. Joo, R. Ryoo, M. Kruk, M. Jaroniec, Z. Liu, T. Ohsuna, O. Terasaki, J. Am. Chem. Soc. 122 (2000) 10712.
[34] S. Li, H. Song, W. Li, X. Ren, S. Lu, G. Pan, L. Fan, H. Yu, H. Zhang, R. Qin, Q. Dai, T. Wang, J. Phys. Chem. B 110 (2006) 23164.